Materials Science and Engineering B 176 (2011) 1277–1284

Contents lists available at ScienceDirect

Materials Science and Engineering B

journal homepage: www.elsevier.com/locate/mseb

Optical properties of ZnO nanowire arrays electrodeposited on *n*- and *p*-type Si(1 1 1): Effects of thermal annealing

O. Lupan [a,*,1], Th. Pauporté [a,*], I.M. Tiginyanu [b], V.V. Ursaki [b], H. Heinrich [c], L. Chow [c]

[a] *Laboratoire d'Electrochimie, Chimie des Interfaces et Modélisation pour l'Energie (LECIME), UMR 7575 CNRS, Chimie ParisTech, 11 rue P. et M. Curie, 75231 Paris, France*
[b] *Institute of Electronic Engineering and Nanotechnologies, Institute of Applied Physics, Academy of Sciences of Moldova, Chisinau MD-2028, Republic of Moldova*
[c] *Department of Physics, University of Central Florida, PO Box 162385 Orlando, FL 32816-2385, USA*

ARTICLE INFO

Article history:
Received 14 April 2011
Received in revised form 21 June 2011
Accepted 11 July 2011
Available online 27 July 2011

PACS:
82.45.Aa
81.15.Pq
82.45.Vp
82.45.Yz
78.67.Uh
68.37.Lp
61.05.C
81.05.Dz

Keywords:
ZnO nanowires
Electrodeposition
Photoluminescence
Annealing
Electrolyte-Si junction
ZnO/Si heterojunction

ABSTRACT

Electrodeposition is a low temperature and low cost growth method of high quality nanostructured active materials for optoelectronic devices. We report the electrochemical preparation of ZnO nanorod/nanowire arrays on *n*-Si(1 1 1) and *p*-Si(1 1 1). The effects of thermal annealing and type of substrates on the optical properties of ZnO nanowires electroplated on silicon (1 1 1) substrate are reported. We fabricated ZnO nanowires/*p*-Si structure that exhibits a strong UV photoluminescence emission and a negligible visible emission. This UV photoluminescence emission proves to be strongly influenced by the thermal annealing at 150–800 °C. Photo-detectors have been fabricated based on the ZnO nanowires/*p*-Si heterojunction.

1. Introduction

ZnO is a II–VI group compound semiconductor with a hexagonal wurtzite crystal structure [1]. It has a wide and direct band gap of 3.37 eV at 300 K and a large free exciton binding energy of 60 meV [1]. Zinc oxide nanowires are the most promising one-dimensional (1D) nanostructures emerging as building blocks for active elements in various nanophotonics systems [2,3]. Low dimensional ZnO has been reported for use in short wavelength optoelectronic devices such as light emitting diodes (LEDs), optical switches, solar cells, field effect transistors, and in nanosensors applications [3–7]. It has unique physical and chemical properties, low-dimensional volume, high aspect ratio, light-matter interaction, cost-effectiveness and can be synthesized by a diversity of chemical and physical methods [3–9]. Among these, electrochemical deposition (ECD) [7,8,10–12] is a low temperature process compatible with different types of substrates [3,4,10] and produces highly crystalline nanowires/nanorods of excellent electronic quality. In this context many device structures, such as heterojunction [3,7,13], homojunction [14], and metal–insulator–semiconductor structure [15] were explored for concrete applications. As ECD can be easily scaled up for optoelectronic device fabrications [3,4,16,17], it is of great interest to develop a process for growing ZnO nanorod/nanowire arrays directly on *n*- and *p*-Si substrates considering the advantages of Si in integrated photodevices.

Recently, Baek and Lim [18] demonstrated the effect of Si wafer resistivity on the growth of ZnO nanorods by using −30 V cathodic potential. The effect of thermal annealing on ECD ZnO nanorod/nanowire arrays is not well documented. Only a few reports [19,20] of annealing effect on ZnO nanorod/nanowire arrays on Si substrates have been published. Ha et al. [20] reported the

* Corresponding authors. Tel.: +33 1 55 42 63 83; fax: +33 1 44 27 67 50.
E-mail addresses: oleg-lupan@chimie-paristech.fr, lupan@mail.utm.md (O. Lupan), thierry-pauporte@chimie-paristech.fr (Th. Pauporté).
[1] On leave from: Department of Microelectronics and Semiconductor Devices, Technical University of Moldova, 168 Stefan cel Mare Blvd., Chisinau, MD-2004, Republic of Moldova.

0921-5107/$ – see front matter © 2011 Elsevier B.V. All rights reserved.
doi:10.1016/j.mseb.2011.07.017

effect of thermal annealing in Ar and O_2 atmosphere on photoluminescence properties of ZnO nanowires grown by thermal vapor on silicon substrate. Liu [21] investigated the effect of annealing on the electrical properties of *n*-ZnO/*p*-Si heterojunction prepared by hydrothermal technique by using a ZnO seed layer deposited by ion beam sputtering technique.

To obtain high optical quality ZnO by ECD it is necessarily to find optimum conditions for growing nanorod/nanowire arrays on Si (in particular, on *p*-type Si) and to study the effect of thermal annealing on their properties. Note that answers to these questions are extremely important for further improvement of the ECD techniques for nanowires-ZnO/*p*-Si photodiodes applications.

In this work, we report the low-potential (≈−1 V) electrodeposition and describe the results of a systematic investigation of the effect of thermal annealing on optical properties of ECD ZnO nanorod/nanowire arrays directly on *n*- and *p*-type Si(1 1 1) substrates. Improvement of structural and optical properties was observed after annealing at 150 °C and 400 °C. *I–V* characteristics of the ZnO nanowires/*p*-Si (1 1 1) heterojunction has been studied. The present paper is driven by the motivation to use ZnO nanorod/nanowire arrays ECD on Si substrates as a practical (ZnO/*p*-Si) heterostructure for silicon based photodiodes with UV sensitivity. These results represent a meaningful step toward fabrication of ZnO/Si devices.

2. Experimental details

2.1. Electrochemical deposition (ECD)

In this work, depositions comprising ZnO nanorod/nanowire arrays were prepared by the cathodic potentiostatic ECD method from the solution containing 0.2 mM $ZnCl_2$ (Merck, 99%). For supporting electrolyte, 0.1 M of potassium chloride KCl (Fluka 98%) was employed to ensure a good conductivity in the aqueous solution [10–12]. The ZnO nanorod/nanowire arrays were grown on the *n*-type Si (1 1 1) and *p*-type Si (1 1 1) substrates with an electrical resistivity of 0.05 and 0.03 Ω cm, respectively. Before electrodeposition the Si substrates were sequentially cleaned by using three steps: solvent clean, RCA clean, and HF dip as reported previously [22–24]. In the solvent clean step, Si wafers were placed in a warm acetone bath (50–53 °C) for 10 min, and then followed by ultrasonic cleaning in DI for 2–3 min. Then, Si wafers were placed in methanol for 4–5 min under ultrasonic cleaning followed by deionized (DI) water (18.2 MΩ cm) rinsing, and then blow dry with air. RCA clean was used to remove organic residues from Si wafers [24] followed by overflowing DI water to rinse and remove the remained solution. Afterwards, the surface was hydrophilic due to the presence of a high density of silanol groups (Si–OH) [25] or to a thin interfacial oxide film. Next, the oxidized substrates were dipped in 2% hydrofluoric acid for 2–3 min to remove silicon dioxide from the Si surfaces, and then thoroughly rinsed in running DI water. Si wafers showed hydrophobicity (not shown) evidenced by water–wafer contact angles at 94° and 95° for *n*-type and *p*-type Si substrates, respectively. These cleaning steps were performed just before the start of the electrodeposition process. Cleaned Si substrate was mounted on a static working electrode with a copper support.

The reference electrode was a saturated calomel electrode (SCE) with a potential at 0.241 V (at 25 °C) vs. NHE (normal hydrogen electrode) which was placed in a separated compartment maintained at room temperature. A platinum spiral wire was used as the counter electrode. The distance between Si working electrode (WE) and counter electrode was 3 cm, and 3.5 cm between the reference electrode and working electrode. Before electrodeposition the electrode surface was again etched for 30 s in 2% HF solution, which gives an atomically smooth (microscopic flatness of the Si surface) and hydrogen terminated surface (hydrophobic), according to previous reports [25–28]. Thus, the silicon surface was mainly covered by Si–H groups [25].

The electrochemical behavior of ZnO was studied using cyclic-voltammetry test performed on *n*- and *p*-type Si (resistivity of 0.05 and 0.03 Ω cm, respectively) before electrodeposition in order to determine optimal cathodic potential for growing process. Electrodeposition was carried out potentiostatically between −0.90 and −1.10 V using an Autolab PGSTAT30 potentiostat/galvanostat monitored by the AutoLab software. The experiment was performed with static WE and with stirring solution (with constant speed of ω = 300 rpm) by a magnetic stirrer. The pH of the solutions was 5.5 initially. The three-electrode electrochemical cell was mounted in a thermo-regulated bath at 90 °C. The electrolyte was saturated with pure oxygen by bubbling for 60 min prior to start electrolysis and continuously bubbled during the growth process. The growing process was performed at constant applied potential and ended in 100 min when the total electrical charge exchanged "per unit area" reached 6.4 C cm^{-2}.

After electrodeposition, zinc oxide nanorod/nanowire arrays were rinsed in DI water to remove un-reacted products from the surface. ECD ZnO was dried in a moderate air flux and then the sample was cut into four equal parts for annealing studies. One piece was used as reference and three other samples were thermal annealed at 150 °C, 400 °C and 800 °C for 1 h in air using a tubular furnace.

2.2. Characterization of ZnO nanorod/nanowire arrays on Si

Phase identification of the ECD ZnO nanorod/nanowire arrays on Si was done with a X-ray diffractometer (XRD) Siemens D5000 (with 40 kV and 45 mA, CuKα radiation with λ = 1.5406 Å). The morphologies of the samples were investigated using a high resolution Ultra 55 Zeiss FEG scanning electron microscope. High-resolution TEM and selected area electron diffraction (SAED) measurements were performed on a FEI Tecnai F30 TEM operating at an accelerating voltage of 300 kV.

The continuous wave (cw) photoluminescence (PL) was excited by the 325 nm line of a Melles Griot He–Cd laser. The emitted light was collected and analyzed with a double spectrometer ensuring a spectral resolution better than 0.5 meV. The signal was detected by a photomultiplier working in the photon counting mode. The laser power for the PL excitation was about 20 mW. The samples were mounted on the cold station of a LTS-22-C-330 optical cryogenic system.

Electrical properties of the thermal annealed ZnO nanowires/Si(1 1 1) heterojunction were studied at room temperature by using a Keithley 2400 digital multi-meter. To investigate the UV response characteristics of the as-grown heterostructure, ohmic contacts were made by using In–Ga eutectic. The UV source used in the photosensitivity responses and current–voltage (*I–V*) characteristics measurements consisted of a source with a peak wavelength of 365 nm. In order to avoid the photoconductivity effect in investigated heterojunction structure ITO/ZnO nanowires/*p*-Si (1 1 1)/In–Ga eutectic, devices were kept in the dark for 3 h before the electrical properties and UV photodetection were explored.

3. Results and discussions

3.1. Electrochemical growth of ZnO on n- and p-type Si electrodes

Fig. 1a and b illustrates the first sweep of cyclic voltammograms (CVs) recorded on bare *n*-type and *p*-type silicon (1 1 1) substrates,

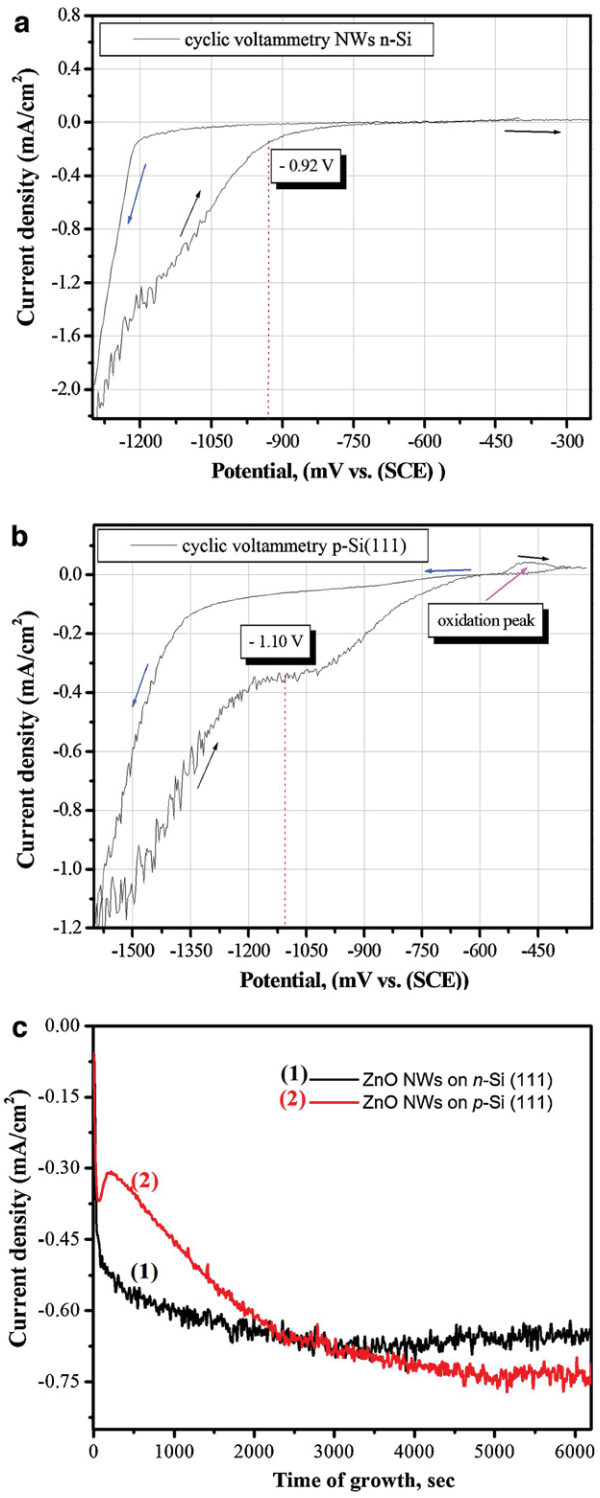

Fig. 1. Cyclic-voltammetry *J–V* characteristics of (a) a *n*-type Si(1 1 1), and (b) a *p*-type Si(1 1 1) electrode in a solution containing 0.2 mM $ZnCl_2$ + 0.1 KCl (pH = 5.5) under oxygen bubbling. (c) Variation of current density with time during ECD of ZnO nanorod/nanowire arrays on (1) *n*-Si(1 1 1) and (2) *p*-Si(1 1 1) substrate at 90 °C, $E = -0.92$ V/SCE (for *n*-Si) and $E = -1.10$ V/SCE (for *p*-Si) with static WE and magnetic stirrer inside the bath, $\omega = 300$ rpm.

respectively. The electrodes are semiconductors that make a Schottky junction with the electrolyte. However, the CV-curves show that the interface is not fully blocking when sufficiently negative potentials are applied to either the *n*-Si or the *p*-Si electrodes. The cathodic current recorded on the negative-going scans is very low for applied potential higher than −1.2 V on *n*-type Si and −1.3 V on *p*-type Si. The behavior is clearly different from that observed on ITO electrodes for instance for which a current onset was observed below −0.9 V [6]. In the present case a marked current onset is found for very negative potential. Since the electrochemical behavior is not significantly different for the two kinds of doping, we can conclude that the oxygen precursor reduction and the ZnO nucleation are difficult on these surfaces. The onset corresponds to the potential for which the nucleation-growth of ZnO on Si starts. Globally the current density is higher on *n*-type Si than on *p*-type Si in spite of the lower resistivity of the *p*-type electrode. Higher current densities are recorded during the positive-going scan with the presence of a shoulder that is more pronounced on the *p*-type electrodes. Also, the reoxydation peak appears in the case of p-Si because the scan boundary is more negative. We also note that on *n*-Si there is no reoxidation peak on the scan, showing that only ZnO was formed over the potential range investigated. A similar observation was found in our previous study on ITO electrode [6]. In the case of the *p*-Si substrate, a small oxidation peak is found in Fig. 1b at about −0.5 V vs. SCE. The hysteresis between the positive and negative scans is due to the nucleation-growth of ZnO and to the change of the chemical nature of the electrode surface which is progressively covered by the zinc oxide. ZnO is deposited according to the reaction [11,12]:

$$Zn^{2+} + \frac{1}{2}O_2 + 2e^- \rightarrow ZnO \quad E_0 = 0.93 \ \text{V/NHE} \tag{1}$$

Different potentials have been tested to find the best values in order to obtain homogeneous well-covering arrays of ZnO nanowires at a low growth rate to improve the quality of the nanostructures [10]. The values presented on the voltammogram (Fig. 1a and b) are −0.92 V and −1.10 V for *n*-type Si and *p*-type Si, respectively. Fig. 1c, curve 1 represents the variation of current density with time for ECD of ZnO nanorod/nanowire arrays on a static *n*-Si substrate at 90 °C, $E = -0.92$ V/SCE in a solution stirred at 300 rpm. The illustrated curve confirms that the ECD ZnO nanorod/nanowire arrays are good electrical conductors, because the current density collected at the electrode is kept at a significant value. Steady state *J* of pure ZnO is about 0.6 mA cm^{-2} after 500 s of growth. Fig. 1c, curve 2 shows the presence of a smaller cathodic wave at short deposition time (<200 s) for *p*-Si substrate. Experimentally, we observed that high quality ZnO nanowire arrays can be grown only at −0.92 V for n-Si and −1.10 V for p-Si substrates, respectively.

The growth process of ZnO nanorod/nanowire arrays on Si can be described by several steps. The electrogeneration of hydroxide ions (OH^-) at the Si surface from oxygen occurs according to the reaction [29,30]:

$$O_2 + 2H_2O + 4e^- \rightarrow 4OH^- \quad E_0 = 0.4 \ \text{V/NHE} \tag{2}$$

This reaction is complex due to the parallel reactions (formation of hydrogen peroxide), whose extent is related to solution and substrate effects, but it presents advantages in terms of process simplicity, controllability, and absence of by-products [30]. Then the growth of ZnO nanorod/nanowire arrays directly on Si can be described by the classical deposition conditions in a chloride medium [16]. Zn(II) is present in the vicinity of the surface, mainly in a $ZnCl^+$ complexed form at a pH close to neutrality [16]. The first steps of growth will be influenced by Zn(II) concentration and the deposition reaction [16]:

$$ZnCl^+ + 2OH^- \rightarrow ZnO_{surf} + H_2O + Cl^- \tag{3}$$

Upon deposition, the interfacial pH increases due to reaction (2). The formation of ZnO nanoparticles in the solution can also take place according to:

$$Zn(II) + 2OH^- \leftrightarrow Zn(OH)_n^{2-n} \rightarrow ZnO_{solut} + H_2O \tag{4}$$

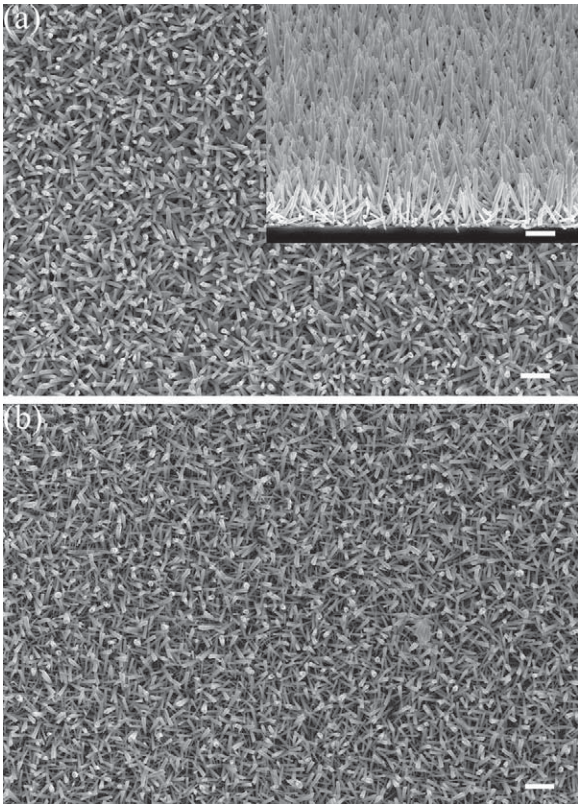

Fig. 2. SEM views of the ZnO nanowires electrodeposited on: (a) *n*-type Si substrate, the inset shows a tilted-view at 65°, and (b) *p*-type Si substrate. Scale bar is 2 μm.

ZnO nanorod/nanowire arrays electrodeposition on Si has been realized under negative polarization to generate the (OH^-) ions and electrostatic interactions must take place between the negatively polarized Si electrode and zinc ion in the solution (Zn^{2+}, $ZnCl^+$ and $Zn(OH)^+$) as was described in details previously [16].

3.2. Structural and morphological-characterizations of ZnO nanowire arrays on Si

The crystal structure and preferential orientation of ZnO nanowires/nanorods on Si substrates were studied by measuring XRD patterns. The XRD patterns from the as-grown ECD ZnO and annealed at 400 °C indicated that we have high quality ZnO nanowires. It can be observed that XRD diffraction peaks are caused by crystalline ZnO with the hexagonal wurtzite structure (space group: $P6_3mc$(186); $a = 0.3249$ nm, $c = 0.5206$ nm). The data are in agreement with the Joint Committee on Powder Diffraction Standards (JCPDS) card for ZnO, Powder Diffraction File No 36-1451. These data are very similar to our previous work [31] and will not be shown here. The full width at half-maximum (FWHM) values of (0 0 2) peaks are 0.12° and 0.16° for the samples as-grown on *n*-type and *p*-type Si, respectively. The lattice constants *a* and *c* were determined as $a = 3.2498$ Å and $c = 5.2066$ Å for pure ZnO [31]. The lattice parameters $c = 5.21 \pm 0.01$ Å and $a = 3.247 \pm 0.005$ Å for ECD ZnO nanorod/nanowire arrays were obtained using standard relations. The unstressed crystal lattice parameters namely $c = 5.207$ Å and $a = 3.250$ Å [27,28] are within that range. The measured value of the *c*/*a* ratio for our sample was 1.604, in agreement with literature value for ZnO, i.e., 1.602.

SEM studies were used to explore the morphology of the as-grown ZnO and the effect of annealing (Fig. 2). The crystal sizes were nearly the same for ZnO before and after annealing, which is in agreement with previous results [32]. It can be seen that

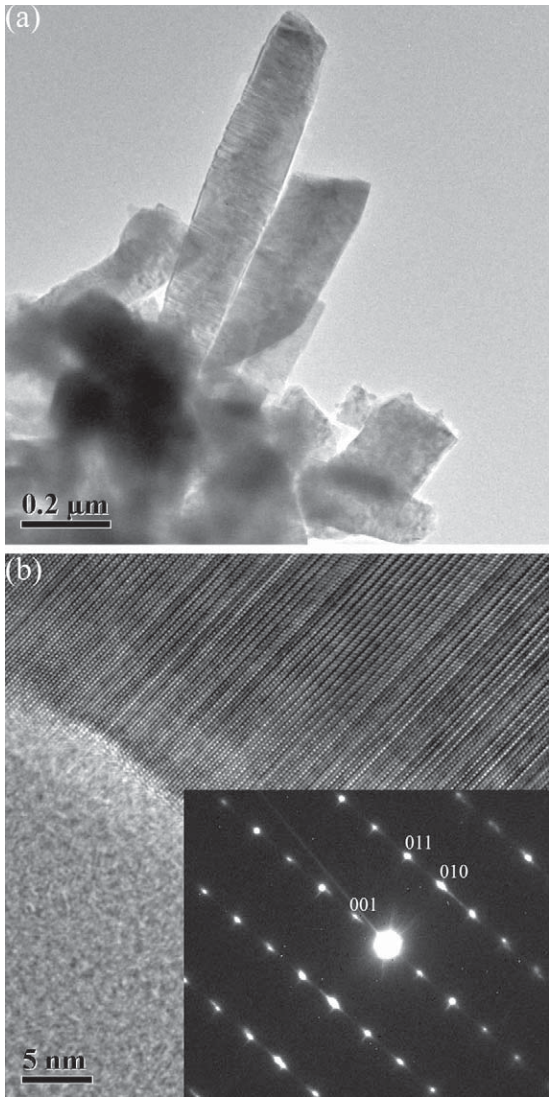

Fig. 3. (a) TEM image from ZnO nanorods, and (b) HRTEM at an edge of the as-synthesized ZnO nanorod and inset is the SAED pattern.

ZnO nanorod/nanowire arrayed crystals fully cover *n*-type and *p*-type Si substrates. The width of the hexagonal faces is about 100–150 nm and their height is in the range 1–2 μm. Growth of the nanorod/nanowire arrays takes place with preferential *c*-axis perpendicular to the Si surface. There is an excellent adherence, and a direct contact/connection between ZnO nanowires and Si substrate (Fig. 2a, inset). The annealing does not induce significant changes in morphology and nanowires sizes.

High resolution transmission electron microscopy (HRTEM) and selected-area electron diffractometry (SAED) were utilized to characterize the microstructure and orientation relationship of the ZnO nanorod/nanowire arrays. The HRTEM images from as-grown ZnO structure on *p*-Si and SAED pattern of ZnO are shown in Fig. 3. In the HRTEM images it can be observed that the nanowire is single-crystalline ZnO with a wurtzite structure grown along the ⟨0 0 1⟩ direction, which is consistent with the XRD results. The SAED pattern (inset of Fig. 3b) clearly reveals highly crystalline material with a hexagonal crystal lattice in this region.

Photoluminescence (PL) studies can provide data related to deep levels (DL), and the ratio I_{UV}/I_{DL} (the intensity of the ultraviolet to the visible deep level related luminescence) is a measure of the quality and defect states in ZnO nanorod/nanowire arrays [32].

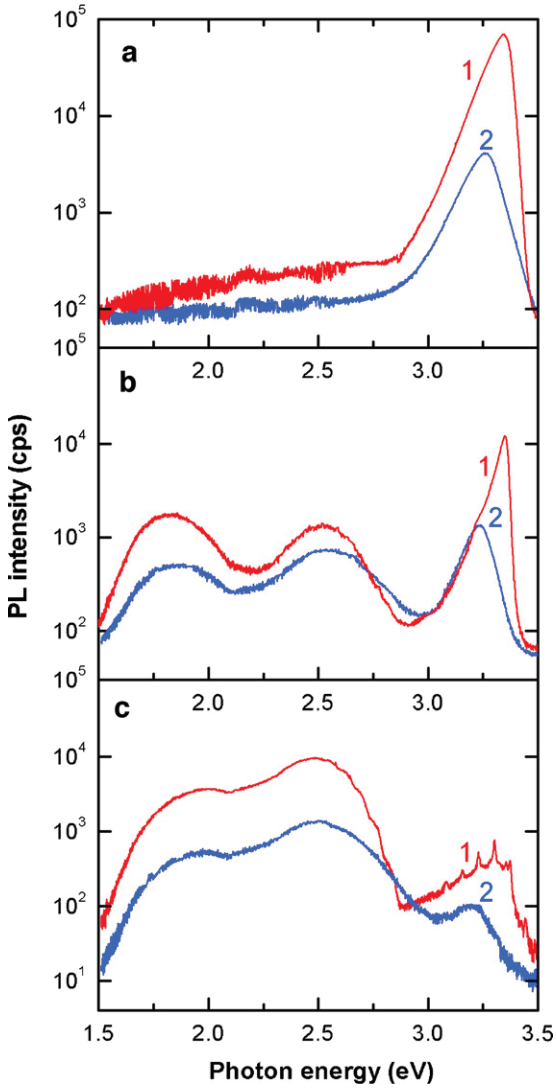

Fig. 4. PL spectra of the as-prepared ZnO sample on (a) *p*-Si, (b) ZnO sample annealed at 400 °C for 1 h in air, and (c) ZnO sample annealed at 800 °C for 1 h in air. The spectra are measured at $T = 10$ K (curve 1), and $T = 300$ K (curve 2).

ZnO nanowires/nanorods on *n*-Si and *p*-Si exhibit similar PL in the visible and UV range. One should note that the ZnO nanowires grown on higher resistivity substrates demonstrate poorer optical quality indicated by a lower intensity of the near bandgap luminescence. It is well-known that the UV photoluminescence is related to the band edge emission while the visible PL is due to defects in the material [33,34] and their peak energy and shape strongly depend on the kind of nanostructures [33,34]. The PL spectrum of the as-prepared samples on *p*-type Si (0.03 Ω cm) (Fig. 4a) consists of a broad intensive near bandgap luminescence with the maximum at 3.345 eV (370.6 nm) at $T = 10$ K and 3.25 eV (381.4 nm) at room temperature. No visible emission is observed. Annealing at 400 °C for 1 h in air leads to decreasing the intensity of the near bandgap luminescence (Fig. 4b) by almost an order of magnitude, a significant narrowing of this PL band, and the emergence of two visible PL bands at 2.55 eV (486.1 nm) and 1.85 eV (670.0 nm). These results can be compared with another effect of thermal annealing on PL properties of ECD ZnO nanorod/nanowire arrays grown on ITO substrate [6]. The effect of annealing on electrodeposited ZnO layers depends on the morphology and the substrate. Indeed, we have found that in the case of dense films grown on ITO [6] or Si [31], the structural quality was markedly improved by the same treatment. This could be due in part to a removal of chloride from the film by annealing, since chloride is present in a larger extend in ZnO films compared to ZnO nanorod/nanowire arrays [34]. In the case of ZnO nanowire arrays epitaxially grown on GaN, the PL was markedly increased after a thermal annealing in air at 300 °C [17]. The increase in the annealing temperature up to 800 °C (Fig. 4c) resulted in a further decrease in the intensity of the near bandgap luminescence by more than an order of magnitude and in a further increase in the visible emission, especially of the band at 1.85 eV.

We will discuss first the possible nature of the near bandgap photoluminescence band in the as-prepared samples. A characteristic feature of this near-band-gap photoluminescence band is the broadening toward the Stokes part of the emission. The width of this PL band in the as prepared sample is 110 meV at 10 K and 155 meV at room temperature. Several mechanisms that may contribute to the broadening of this PL band have been previously discussed [32,35–37]. It was shown that most probably this PL band is due to direct transitions of electrons from the conduction band tails to valence band tails. The broadening of the PL band involved can be accounted for by the broadening of the band edges due to potential fluctuations induced by the high concentration of intrinsic defects or impurities. The width of the band tails, and the dependence of the FWHM of the PL band on carrier concentration, can be calculated using the model for broadening of impurity bands in heavily doped semiconductors developed by Morgan [38]. This model has been applied to correlate the width of the PL band to the free carrier concentration in highly doped ZnO samples [32,35–37]. By using the established dependence, one can estimate that the electron concentration in as-prepared sample to be 1.3×10^{20} cm^{-3} at $T = 10$ K, and 2.6×10^{20} cm^{-3} at room temperature. Note that with such a high concentration of free carriers no distinct excitonic lines are observed in the PL spectrum, which usually are observed in crystals with a lower degree of doping.

As concerns the microscopic origin of the impurity responsible for the potential fluctuations, one can assume that it is related to unintentionally introduced doping impurity, or/and to intrinsic defects caused by the deviation from stoichiometry. Oxygen vacancies and zinc interstitials are the most probable donor-type intrinsic defects [39,40]. Oxygen vacancy is a deep donor, while zinc interstitial is a shallow one [39]. Thus, interstitial zinc Zn_i defects can also contribute to the high electron concentration.

The temperature dependences of the near bandgap PL spectra in as-prepared and annealed samples are shown in Fig. 5. Annealing at 400 °C leads to narrowing of the near bandgap photoluminescence peak. The maximum of the PL band is situated at 3.355 eV (369.5 nm) at 10 K, and 3.23 eV (383.8 nm) at room temperature, while its full width at half maximum (FWHM) is 46 meV at 10 K and 126 meV at 10 K and room temperature, respectively. One can estimate from these data that the electron concentration is 2.6×10^{19} cm^{-3} at $T = 10$ K, and 1.7×10^{20} cm^{-3} at room temperature. However, one cannot exclude some errors in estimation of the free carrier concentration in the sample annealed at 400 °C due to the deviation of the recombination mechanism from the Morgan model, indicated by the emergence of a low energy shoulder in the contour of the emission spectrum of this sample.

We found that annealing at 800 °C led to a spectacular decrease of the near bandgap photoluminescence intensity accompanied by a low-energy shift of the PL band and its significant broadening. This makes possible the determination of the resonant Raman scattering (RRS) lines in the emission spectra. Note that typically up to 6 overtones are observed in the RRS spectrum of unintentionally doped ZnO samples [32,35,36], while up to 10 LO phonon lines are clearly seen in Fig. 5c. A similar effect has been previously observed in ZnO nanorods doped with Cu or Ni, as well as in samples co-doped with Mn and Co [41]. The enhancement of RRS is attributed

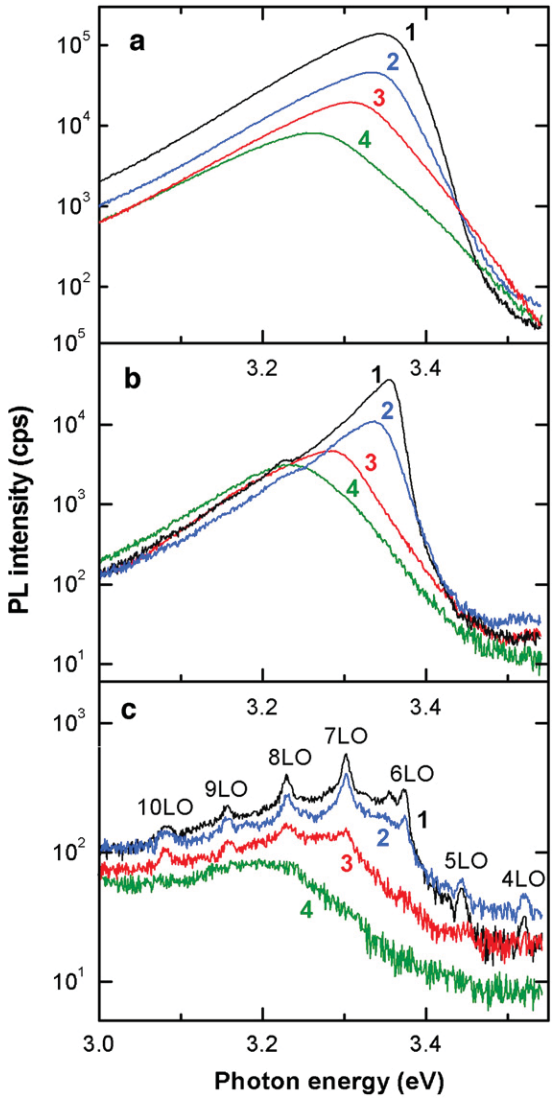

Fig. 5. (a) Near bandgap PL spectra of the as-prepared sample on *p*-Si, (b) ZnO sample annealed at 400 °C for 1 h in air, and (c) ZnO sample annealed at 800 °C for 1 h in air. The spectra are measured at $T = 10$ K (curve 1), $T = 100$ K (curve 2), $T = 200$ K (curve 3), and $T = 300$ K (curve 4).

to correlations between the RRS and the red-shifted PL line due to intrinsic and extrinsic defects [41]. The increase of the concentration of defects upon annealing at 800 °C is also indicated by the increase in the intensity of visible luminescence.

The different behavior of the defects responsible for the high concentration of electrons and those responsible for the visible luminescence with increasing the annealing temperature is indicative of their different microscopic origin. One can suggest that the decrease of the electron concentration is due to the formation of some complexes with the impurities or Zn_i defects responsible for the high electron concentration. Another possibility is the out-diffusion of these impurities or defects with increasing the annealing temperature. On the contrary, annealing may result in the increase of the concentration of defects responsible for the visible emission, which is usually associated with complexes of zinc vacancies, oxygen vacancies, or interstitial oxygen.

Taking into account the *n*-type conductivity of the produced material, one can suggest that the assignment of these PL bands to the electron transitions from a deep donor level to the valence band (*D*-*h*-type recombination) is very improbable [42]. Most probably, these PL bands are due to electronic transitions from the conduction band to acceptor levels (*e*-*A*-type recombination). The red band at 1.85 eV is supposed to be associated with a deep unidentified acceptor A_1 with the energy level situated close to the middle of the bandgap [43]. The PL band at 2.55 eV is most probably due to zinc vacancy V_{Zn} acceptor center A_2. Zinc vacancy is expected to have charge −2 in *n*-type ZnO where its formation is more favorable. The transition level between the −1 and −2 charge states of V_{Zn} occurs at ∼0.8 eV above the valence band [43]. Thus, one may expect transitions from the conduction band to the V_{Zn} acceptor at around 2.6 eV in *n*-type ZnO. The scheme of energy levels and electronic transitions responsible for the PL bands observed is presented in Fig. 6.

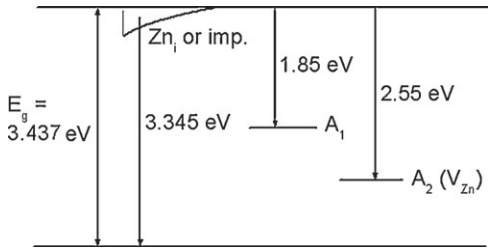

Fig. 6. Scheme of energy levels and electronic transitions responsible for the PL bands.

The FWHM of the PL band in as-prepared samples and samples annealed at 400 °C as a function of temperature is shown in Fig. 7a, while Fig. 7b presents the Arrhenius plot of the free electron concentration deduced from the FWHM of the PL band according to the Morgan modes as mentioned above. The activation energy estimated from the high temperature slope of the Arrhenius plot assuming that the semiconductor is non-compensated is around 100 meV. On the other hand, from the position of the PL band maximum in the sample annealed at 400 °C (3.355 eV) taking into account the value of the ZnO bandgap at low temperature (3.437 eV) one can estimate an activation energy of 82 meV. This difference could be due to a partial compensation of conductivity, as well as due to the deviation of the recombination mechanism from the Morgan model.

3.3. Applications to UV-photodetectors

The ZnO nanowire arrays prepared by electrodeposition have been included in a heterojunction structure ITO/ZnO nanowires/*p*-Si (1 1 1)/In–Ga as illustrated in the inset of Fig. 8. The current–voltage (*I*–*V*) characteristic curves of the diode obtained are displayed in Fig. 8. Under dark conditions, a threshold voltage of about 0.5 V and a typical rectifying character is found. However, the heterojunction has a fairly low threshold and reverse breakdown voltage value. The relatively low threshold breakdown voltage in all probability is due to the more likely tunneling current in heavy doped (p^+)-Si [42]. A UV-source at 365 nm was used to test the photosensitivity of the diode at short wavelengths by measuring the current–voltage (*I*–*V*) characteristics under illumination. A marked response was found at forward bias above the threshold voltage. No pronounced degradation in the heterojunction properties after overheating in normal ambient was observed. More details on ZnO nanowires/*n*,(*p*)-Si (1 1 1) heterostructures-based photodetectors will be presented in a forthcoming paper. We can also note that we have shown recently that the structure acts as a visible light emitting diode when biased at higher forward voltage [43].

4. Conclusions

ZnO nanorod/nanowire arrays were deposited directly on *n*-type and *p*-type silicon (1 1 1) substrates using a low temperature

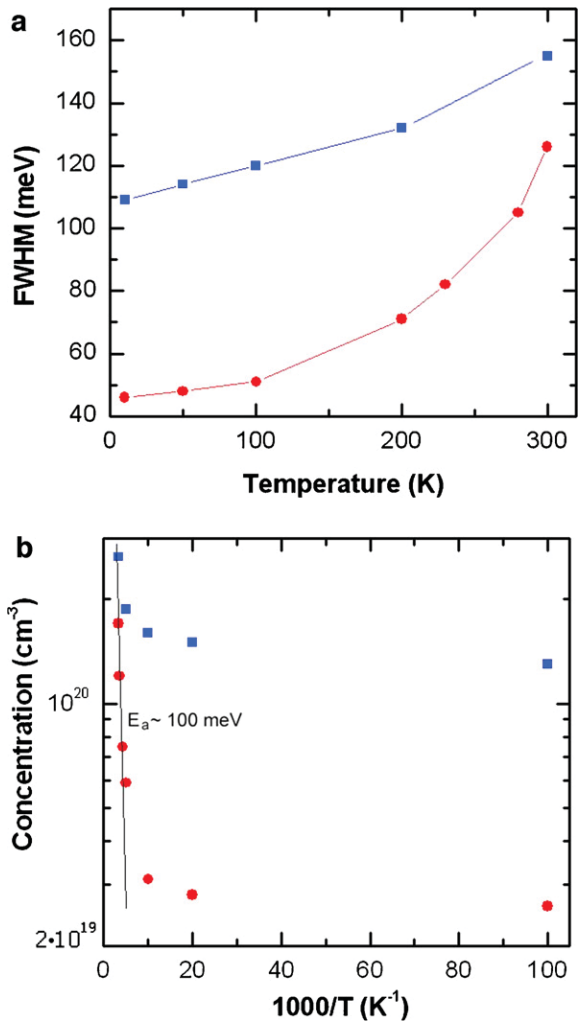

Fig. 7. (a) FWHM as a function of temperature and (b) free electron concentration as a function of $1/T$ for as prepared samples on *p*-Si (blue squares) and samples annealed at 400 °C for 1 h in air (red circles). (For interpretation of the references to color in this figure legend, the reader is referred to the web version of the article.)

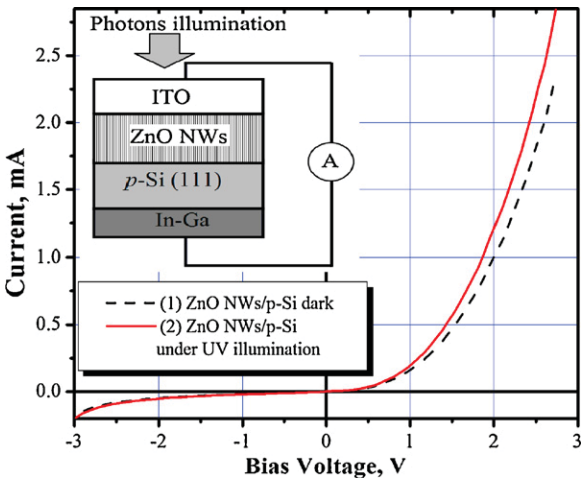

Fig. 8. Current–voltage (*I–V*) characteristics of the as-grown ZnO nanowires/*p*-Si (1 1 1) heterojunction. The inset is the schematic cross-sectional view of the ZnO nanowires/*p*-Si (1 1 1) heterojunction-based photodetector/photodiode.

electrochemical method at low voltage. To grow ZnO on *n*- and *p*-Si substrates we determined the values of the cathodic potential which allow both reaction and deposition. The reaction steps for the growth of ZnO nanowire arrays on Si have been described, the formation and diffusion of electrogenerated hydroxide ions (OH^-) at the Si surface being explained. From SEM, we observed that ZnO nanorod arrays fully cover *n*-type and *p*-type Si substrates. The width of the nanorod/nanowire arrays is about 100–150 nm and their height is in the range 1–2 μm. The high-resolution TEM and SAED are indicative of crystallinity of ZnO nanorod/nanowire arrays with a hexagonal crystal lattice [44].

ZnO nanorod/nanowire arrays were found to exhibit similar PL in the UV region for samples grown on *n*-type or *p*-type silicon (1 1 1). The PL spectrum of the as-prepared samples consists of a broad and very intensive near bandgap band with the maximum at 3.345 eV at $T = 10$ K and 3.26 eV at room temperature. No visible emission is observed in the sample. Annealing at 400 °C for 1 h in air lead to a decrease in the intensity of the near bandgap luminescence by almost an order of magnitude, significant narrowing of this PL band and the emergence of two visible PL bands at 2.55 eV and 1.85 eV. The heterojunction structure ITO/ZnO nanowires/*p*-Si (1 1 1)/In–Ga shows a response to UV light at room temperature. This encouraging result suggests that ZnO nanowires/Si heterostructures can be further explored for devices applications, such as photodetectors.

References

[1] H.E. Brown, J. Phys. Chem. Solids 15 (1960) 86.
[2] (a) Z.L. Wang, J. Nanosci. Nanotechnol. 8 (2007) 27;
(b) Z.L. Wang, Mater. Sci. Eng. R 64 (2009) 33.
[3] O. Lupan, T. Pauporté, B. Viana, Adv. Mater. 22 (2010) 3298–3302.
[4] T. Pauporté, Design of solution-grown ZnO nanostructures, in: Z.M. Wang (Ed.), Lecture Notes on Nanoscale Science and Technology, Toward Functional Nanomaterials, vol. 5, Springer Books, New York, 2009, pp. 77–125.
[5] L. Luo, Y. Zhang, S.S. Mao, L. Lin, Sens. Actuators A: Phys. 127 (2006) 201.
[6] O. Lupan, V.M. Guérin, I.M. Tiginyanu, V.V. Ursaki, L. Chow, H. Heinrich, T. Pauporté, J. Photochem. Photobiol. A: Chem. 211 (2010) 65–73.
[7] T. Pauporté, D. Lincot, B. Viana, F. Pellé, Appl. Phys. Lett. 89 (2006) 233112.
[8] C. Badre, T. Pauporté, M. Turmine, D. Lincot, Nanotechnology 18 (2007) 365705.
[9] N. Wang, Y. Cai, R.Q. Zhang, Mater. Sci. Eng. R 60 (2008) 1–51.
[10] T. Pauporté, D. Lincot, Appl. Phys. Lett. 75 (1999) 3817.
[11] A. Goux, T. Pauporté, J. Chivot, D. Lincot, Electrochim. Acta 50 (2005) 2239.
[12] T. Pauporté, D. Lincot, J. Electroanal. Chem. 517 (2001) 54.
[13] Y.I. Alivov, E.V. Kalinina, A.E. Cherenkov, D.C. Look, B.M. Ataev, A.K. Omaev, M.V. Chukichev, D.M. Bagnall, Appl. Phys. Lett. 83 (2003) 4719.
[14] J.H. Lim, C.K. Kang, K.K. Kim, I.K. Park, D.K. Hwang, S.J. Park, Adv. Mater. 18 (2006) 2720.
[15] Y.I. Alivov, D.C. Look, B.M. Ataev, M.V. Chukichev, V.V. Mamedov, V.I. Zinenko, Y.A. Agafonov, A.N. Pustovit, Solid-State Electron. 48 (2004) 2343.
[16] H.El. Belghiti, T. Pauporté, D. Lincot, Phys. Status Solidi 205 (2008) 2360.
[17] O. Lupan, T. Pauporté, B. Viana, I.M. Tiginyanu, V.V. Ursaki, R. Cortés, Appl. Mater. Intefaces 2 (2010) 2083–2090.
[18] S. Baek, S. Lim, Thin Solid Films 517 (2009) 4560.
[19] C. Liu, Y. Masuda, Y. Wu, O. Takai, Thin Solid Films 503 (2006) 110–114.
[20] B. Ha, H. Ham, C.J. Lee, J. Phys. Chem. Solids 69 (2008) 2453–2456.
[21] S.Y. Liu, J. Appl. Phys. 105 (2009) 114504.
[22] W. Kern, J. Vossen (Eds.), Thin Film Processes, Academic Press, New York, 1978 (Ch V-1);
Reinhardt, A. Karen, W. Kern (Eds.), Handbook of Silicon Wafer Cleaning Technology, 2nd edition, William Andrew, Norwich, NY, USA, 2008.
[23] S.T. Shishiyanu, O.I. Lupan, T.S. Shishiyanu, V.P. Şontea, S.K. Railean, Electrochim. Acta 49 (2004) 4433.
[24] W.A. Kem, D.A. Puotinen, RCA Rev. 31 (1970) 187.
[25] Lehmann, Volker Electrochemistry of Silicon: Instrumentation, Science, Materials and Applications, Wiley-VCH Verlag GmbH, D-69469, Weinheim, 2002.
[26] R.C. Henderson, J. Electrochem. Soc. 119 (1972) 772.
[27] S.I. Raider, R. Flitsch, M.J. Palmer, J. Electrochem. Soc. 122 (1975) 413.
[28] E.A. Dalchielle, P. Giorgi, R.E. Marotti, F. Martn, J.R. Ramos-Barrado, R. Ayouci, D. Leinen, Sol. Energy Mater. Sol. Cells 70 (2001) 245–254.
[29] T. Pauporté, D. Lincot, Electrochim. Acta 45 (2000) 3345.
[30] A. Goux, T. Pauporté, D. Lincot, Electrochim. Acta 51 (2006) 3168.
[31] O. Lupan, Th. Pauporté, V.V. Ursaki, I.M. Tiginyanu, Opt. Mater. 33 (2011) 914–919.
[32] V.V. Ursaki, O.I. Lupan, L. Chow, I.M. Tiginyanu, V.V. Zalamai, Solid State Commun. 143 (2007) 437.
[33] W.D. Yu, X.M. Li, X.D. Gao, Appl. Phys. Lett. 84 (2004) 2658.

[34] T. Pauporté, E. Jouanno, F. Pellé, B. Viana, P. Aschehoug, J. Phys. Chem. C 113 (2009) 10422.
[35] V.V. Ursaki, I.M. Tiginyanu, V.V. Zalamai, E.V. Rusu, G.A. Emelchenko, V.M. Masalov, E.N. Samarov, Phys. Rev. B 70 (2004) 155204.
[36] V.V. Zalamai, V.V. Ursaki, E.V. Rusu, P. Arabadji, I.M. Tiginyanu, L. Sirbu, Appl. Phys. Lett. 84 (2004) 5168.
[37] E. Iliopoulos, D. Doppalopudi, H.M. Ng, T.D. Moustakas, Appl. Phys. Lett. 73 (1998) 375.
[38] T.N. Morgan, Phys. Rev. 139 (1965) A343.
[39] S.B. Zhang, S.H. Wei, A. Zunger, Phys. Rev. B 63 (2001) 075205.
[40] E. Oba, S.R. Nishitani, S. Isotani, H. Adachi, I. Tanaka, J. Appl. Phys. 90 (2001) 824.
[41] T.L. Phan, R. Vincent, D. Cherns, N.X. Nghia, V.V. Ursaki, Nanotechnology 19 (2008) 475702.
[42] H. Sun, Q.F. Zhang, J.L. Wu, Nanotechnology 17 (2006) 2271.
[43] O. Lupan, T. Pauporté, B. Viana, J. Phys. Chem. C 114 (35) (2010) 14781.
[44] L. Chow, O. Lupan, H. Heinrich, G. Chai, Appl. Phys. Lett. 94 (16) (2009) 163105.